

Algebraic law of local correlation in the dynamically tuned Ising model

Xin Wang,¹ Xiaofeng Wu,¹ Bo Yang,² Bo Zhang,¹ and Bo Xiong^{1,*}

¹Department of Physics, Wuhan University of Technology, Wuhan 430070, China

²School of Mathematics and Physics, Hubei Polytechnic University, Huangshi 435003, China

(Dated: December 5, 2024)

We investigate both analytically and numerically the buildup of antiferromagnetic (AF) correlation in the dynamically tuned Ising model with various geometries by using the Rydberg atomic system. It is shown that Magnus expansion up to second order for the local lattice geometries can describe quantitatively the creation of the AF correlation for different lattice arrays, e.g., $2 \times n$ lattice, cyclic lattice with star, and triangular lattice. We find that the magnitude of AF correlation for the same Manhattan distance is the algebraic sum of the correlations contributed by all shortest paths — a typical superposition law. Such a law is independent of nonequivalent paths, lattice geometries, and quench style.

Understanding nonequilibrium dynamics of complex, strongly interacting many-body systems is an important and challenging issue at the intersection between statistical physics and quantum physics [1, 2]. The crucial part of such dynamics is to explore the buildup of inner correlations and its time evolution in these systems, especially in the regime of quantum phase transition. Previous theoretical works focus on understanding the density of topological defects [3–5] through Kibble-Zurek mechanism, Landau-Zener formula and mean-field theory, and also the quantum fluctuations [6] based on mean-field expansion when the system with uniform interactions is driven through the critical point at a finite rate. However, for a nonuniform system and due to the exponential growth of Hilbert space with the number of grids and particles, it is extremely hard to study the temporal variation of the local or long-ranged correlation by both analytic treatment and numerical simulation. Therefore, to develop efficient theory for the nonequilibrium dynamics of the *nonuniform* system is immediately necessary for understanding essentially the buildup mechanism of the inner correlation [7, 8] and characteristic dynamics [9–11] and also has broad implications in quantum simulation [12, 13] and quantum information [14].

Experiments have employed Rydberg atoms to realize some lattice arrays with various geometries, such as triangular lattice [8, 13], Kagome lattice [15, 16], honeycomb lattice [17], and even microstructure with several atoms including the star, cyclic, diamond, and hexagon graph [18]. Owing to its strongly controllable experimental parameters, e.g., atomic interaction and Rabi frequencies [12, 19], it provides a versatile quantum simulation platform to investigate the nonequilibrium dynamics of strongly interacting many-body system in various array geometries. In this letter, we consider the dynamically tuned nonuniform Ising model with various lattice geometries, which can be realized by Rydberg atomic system. By employing Magnus expansion (ME), we derive the analytic expression of the connected correlation function and capture the essential features of the buildup of AF correlation for such system. We find the superposition law of the local correlation; specifically, the magnitude of AF correlation for the same Manhattan distance is the algebraic sum of all shortest paths. The superposition law is preserved even though the shortest paths are

not equivalent, indicating lattice geometries have less effect on such a law. Consequently, to probe the buildup of correlations for complex lattice geometries can be simplified to investigate simple lattice units. This type of superposition is subsequently shown to be immune against quench style. Finally, these findings are verified by numerically solving Schrödinger equations for these system with various size.

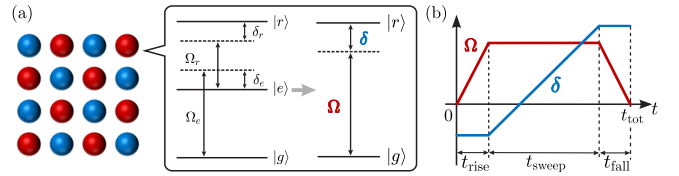


FIG. 1. (a) Schematic description of the lattice, and atoms are excited from the ground state $|g\rangle$ to the Rydberg state $|r\rangle$ through a two-photon process. (b) The protocol of Rabi frequency $\Omega(t)$ and detuning $\delta(t)$.

Recently there are a variety of experiments to investigate nonequilibrium dynamics by manipulating the Rydberg atoms in optical lattice or optical tweezers [8, 11]. In these experiments, atoms are initially prepared in the ground state $|g\rangle$ and then coupled to the Rydberg state $|r\rangle$ by a two photon optical transition with an effective Rabi frequency $\Omega = \frac{\Omega_e \Omega_r}{2\delta_e}$ and detuning $\delta = \delta_e + \delta_r + \frac{(\Omega_e^2 - \Omega_r^2)}{4\delta_e}$ [Fig. 1 (a)]. Owing to a strong, repulsive van der Waals interaction $U_{ij} \sim 1/r_{ij}^6$, atoms within a critical distance can not occupy simultaneously $|r\rangle$; this is a so-called Rydberg blockade [20]. Here we consider the Rydberg blockade radius $R_b \cong r_{(ij)}$, where the adjacent atoms are hardly excited simultaneously to $|r\rangle$. Such system can be described by the Hamiltonian

$$H = \frac{\hbar\Omega(t)}{2} \sum_i \sigma_i^x - \hbar\delta(t) \sum_i n_i + \sum_{\langle ij \rangle} U_{ij} n_i n_j, \quad (1)$$

where $\sigma_i^x = |r\rangle\langle g|_i + |g\rangle\langle r|_i$ is the x -Pauli matrix, which refers to transition operator at site i between the ground state $|g\rangle$ and the Rydberg state $|r\rangle$. $n_i = |r\rangle\langle r|_i$ denotes the projector operator of the Rydberg state for atom i , which is related to the z -Pauli matrix by $n_i = \frac{(\sigma_i^z + 1)}{2}$. The Hamiltonian (1) is regarded

as the quantum Ising model where a transverse field $B_{\perp} \propto \Omega$, a longitudinal field $B_{\parallel} \propto \delta$ and Ising coupling U_{ij} . The associated equilibrium state for $U > 0$ displays two phases, paramagnetic (PM) and antiferromagnetic phases, with a second-order phase transition between them. The PM and AF phases are respectively referred to the states in the magnetic systems where spins are not ordered and adjacent spins are arranged in an antiparallel structure.

To explore the buildup of AF correlation, we employ the quench protocol shown in Fig. 1 (b) similar to the experiments [8]. Starting with all atoms in $|g\rangle$, we slowly switch on Ω with a ramping-up time of t_{rise} until $\Omega = \Omega_{\text{max}}$ with a negative constant detuning of δ_0 . Afterwards, we fix Ω with duration time t_{sweep} and modulate δ to increase linearly from δ_0 to a positive value δ_f where the parameters come into the region of the AF phase. Subsequently, Ω is slowly switched off with a ramping-down time of t_{fall} while δ is unchanged. The buildup of the AF correlation in such process can be measured by the connected spin-spin correlation,

$$C_{kl} = \frac{1}{N_{kl}} \sum_{(ij)} [\langle n_i n_j \rangle - \langle n_i \rangle \langle n_j \rangle] \quad (2)$$

where the sum is taken over atom pairs (ij) that exist the same relative separations $\mathbf{r}_i - \mathbf{r}_j = (ka, la)$, and the numbers of these pairs in the lattice geometry is denoted as N_{kl} . Also a denote the relevant separations between two atoms in horizontal and vertical directions in the system with nonuniform interactions. Nonuniform interactions between Rydberg atoms can be realized experimentally by controlling precisely the intensity and orientation of the external field besides adjusting the distance between two atoms [21, 22].

The nonequilibrium dynamics of the Ising-like model is conventionally inaccessible to explore analytically due to the growth scale in size of Hilbert space for a large number of particles. However, for locally interacting systems with finite local degrees of freedom on n -hypercubic lattices, exact solutions become feasible [23]. Here, in finite time scale where many-body system does not become chaos or thermalized, we employ ME to derive analytic expression for some quantities, e.g., the connected correlation function, and compare it with exactly numerical solutions. ME is a practical way to build up approximate exponential representations of the solution of linear systems of differential equations with varying coefficients [24]. It has been applied widely in some areas, from atomic and molecular physics [25, 26] to nuclear magnetic resonance [27] to quantum electrodynamics and elementary particle physics [28, 29].

In the treatment of ME, the matrix exponential of many-body propagator yields $\hat{U}(T) = \exp[-iT\hat{H}(T)]$, where $\hat{H}(T)$ is a series expansion for the matrix associated to nested commutators of the time-dependent Hamiltonian (1), i.e., $\hat{H}(T) = \sum_{k=1}^{\infty} \hat{H}_k(T)$. To avoid some unwieldy terms involved in the calculation, we consider the ME up to second-order terms and truncate higher-order expansion $\hat{H}_1 = \frac{1}{T} \int_0^T H(t_1) dt_1$ and $\hat{H}_2 = \frac{i}{2T} \int_0^T \left[\int_0^{t_1} H(t_2) dt_2, H(t_1) \right] dt_1$,

where the communication of operators fulfills $[\hat{A}, \hat{B}] = \hat{A}\hat{B} - \hat{B}\hat{A}$. About the rigorous proof of the self-consistency of ME, e.g., for $U = 0$, $C_{kl} = 0$, is shown in the supplemental material [30]. One may note that there exists an internal connection between Magnus series and Dyson perturbative series. The former derives the integral of the nested commutators due to the nonzero anticommutation of the Hamiltonians at different times and the latter causes the path integral raised by the time-order products.

We first consider the experimentally accessible case, a linearly modulating detuning $\delta(t) = \frac{\delta_f - \delta_0}{T}t + \delta_0$, where δ_0 is the original value and δ_f is the final value of the detuning. One can deduce straightforwardly ($\hbar = 1$), $\bar{H}_1 = \frac{\Omega}{2} \sum_i \sigma_i^x - \delta_{\text{avg}} \sum_i n_i + \sum_{(ij)} U_{ij} n_i n_j$ and $\bar{H}_2 = \frac{\Omega}{24} (\delta_f - \delta_0) T \sum_i \sigma_i^y$ with $\delta_{\text{avg}} = \frac{\delta_0 + \delta_f}{2}$. Note that the final term in \bar{H} is linearly dependent on T , which is originated from the second-order ME. Under the condition that $\int_0^T \|H(t)\|_2 < \pi$, where $\|H\|_2$ is the euclidean norm of H defined as the squared root of the largest eigenvalue of positive semi-definite operator $H^\dagger H$, we can expand the matrix exponential into $\hat{U}(T) = \sum_{n=1}^{\infty} \frac{(-iT)^n}{n!} \bar{H}^n(T)$, where the high-power terms in T appear and will contribute in the following correlation function.

To explore the effect of paths between the grid point $(0, 0)$ and (ka, la) in the buildup of AF correlation, we utilize $C_R(T) = C_{((0,0),(k,l))}$ where the Manhattan distance $R = |k| + |l|$. In the treatment of Magnus approach to the Ising-like Hamiltonian, the buildup of the AF correlation characterised by $C_R(T)$ requires the expansion of exponential matrix $\hat{U}(T)$ in sufficiently high powers where the interaction term plays a significant role in the dynamic process. We stress that the non-zero anticommutation of the Hamiltonian at different time in \bar{H}_2 is the essential part in the ME, so it should be taken into account to obtain more accurate results. By using the ME up to second-order, C_R is divided into three parts, i.e., $C_R = C_R^{\text{Path}} + C_R^{\text{Coupling}} + C_R^{\text{Time}}$, where C_R^{Path} , C_R^{Coupling} , and C_R^{Time} denote the contribution from the shortest paths, the nearest-neighbor coupling for the shortest paths, and the mutual effect of the Hamiltonian at different times, respectively. In general, a graphic description about the analytic results of C_R for the nearest-neighbor sites and the next-nearest-neighbor sites has the feature,

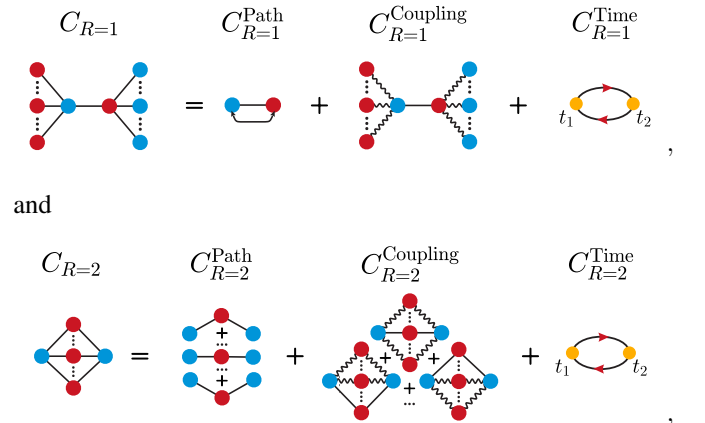


TABLE I. Parameters used for the numerical and analytic results presented in the main text.

Figures	Structures	$U_1/h(\text{MHz})$	$U_2/h(\text{MHz})$	$U_3/h(\text{MHz})$	$\Omega_{\max}/(2\pi)(\text{MHz})$	$\delta_f/(2\pi)(\text{MHz})$
2 (a),3	$2 \times n$ lattice	2.8	1.4	/	1.8	[1, 7]
2 (b)	cyclic lattice with star	2.8	1.4	3.0	0.8	[1, 5]
2 (c)	triangular lattice	2.7	/	/	0.8	[1, 5]

where the solid lines between two reference balls label the shortest paths and the wave lines denote the coupling from the nearest-neighbor sites to the shortest paths. Such method has captured the buildup of AF correlation for dynamically tuned Ising-like model with uniform interaction in agreement with exactly numerical calculation [31].

We employ both ME and numerical simulation for three geometries with periodic boundary conditions in the row — the $2 \times n$ lattice, the cyclic lattice with star, and the triangular lattice, to investigate (I) the influence of the nonuniform interaction in the buildup of AF correlation, (II) the validity of algebraic law or superposition principle for C_R in accordance with nonequivalent paths, (III) the analytic description of the AF buildup for a frustrated magnetic system. About the detailed deduction of C_R from ME for these lattice arrays and its accuracy verified by numerical results, please see [30]. The numerical results are based on fourth-order Runge-Kutta [32] for various lattice size. We find that in the current time scale, the numerical calculation shows similar results of the connected correlation functions for different lattice lengths, e.g., 2×8 , 2×10 , 2×12 for $2 \times n$ lattice. The typical parameter values $\Omega_{\max}/(2\pi)$, $\delta_f/(2\pi)$ and $U_i/h(i = 1, 2, 3)$ for our calculation is shown in Table. I.

To investigate the influence of nonequivalent paths in the buildup of AF correlation, we begin to consider 2×12 lattice array where $U_1 = 2U_2 = h \times 2.8\text{MHz}$ [see Fig. 2 (a1)]. Such nonuniform interactions induce two types of $C_{R=1}$, i.e., $C_{10,\text{square}}$ and $C_{01,\text{square}}$. In Fig. 2 (a2), $|C_{10,\text{square}}| > |C_{01,\text{square}}|$ for the same δ_f , indicating that in the quench process, a larger interaction U_1 tends to enhance the AF correlation. Meanwhile, our analytic results about $C_{R=1}$ agree quantitatively with numerical ones. Note that any absence of $C_{R=1}^{\text{Path}}$, $C_{R=1}^{\text{Coupling}}$, and $C_{R=1}^{\text{Time}}$ in the ME can not give $C_{R=1}$ close to numerical calculation [see [30]]. Furthermore, we find that $C_{10,\text{square}}^{\text{Path/Time}}$ have the forms, identical to $C_{01,\text{square}}^{\text{Path/Time}}$, indicating that the shortest path and the mutual effect of Hamiltonian at different times contribute equivalently to the AF correlations in the two structures. The critical difference of two correlation functions originates from the nearest-neighbor coupling for the shortest path, $C_{R=1}^{\text{Coupling}}$. Such discrepancy is raised by the mutual effect of the coupling Ω in the nearest-neighbor sites to the shortest path and the interaction U between the shortest path and its nearest-neighbor sites, which corresponds naturally to the differences of lattice geometries. Therefore, it emphasizes the importance of the coupling from the nearest-neighbor sites to the shortest path for buildup of AF correlations in various lattice geometries and the necessary of

considering $C_{R=1}^{\text{Coupling}}$ in the ME.

In the calculation of $C_{R=2}$, ME provides the double relation between $C_{11,\text{square}}$ and $C_{20,\text{square}}$, where $C_{11,\text{square}}^{\text{Path/Time}} = 2 \times C_{20,\text{square}}^{\text{Path/Time}}$ and $C_{11,\text{square}}^{\text{Coupling}} \approx 2 \times C_{20,\text{square}}^{\text{Coupling}}$. This relation has been verified by our numerical calculation [see Fig. 2 (a3) and Fig. 2 (a4)]. Such an agreement indicates that despite more complex paths are involved for $C_{R=2}$ than $C_{R=1}$, the buildup of the AF correlation in a finitely large lattice array is still governed by its local structure around the correlated sites. The key factor for $C_{11,\text{square}} = 2 \times C_{20,\text{square}}$ is originated from the fact that only one shortest path contributes to $C_{20,\text{square}}$ while there are two shortest paths for $C_{11,\text{square}}$. Therefore, it implies that there exists a superposition law: the magnitude of the connected correlation function for two reference points is the algebraic sum of the correlations contributed by all its shortest paths.

To explore more the effect of nonequivalent paths on the spatial correlations, we consider the geometry of the cyclic lattice where $U_1/h = 2U_2/h = 2.8\text{MHz}$ and $U_3/h = 3.0\text{MHz}$ [see Fig. 2 (b1)]. These nonuniform interactions give rise to four types of $C_{R=2}$, i.e., $C_{20,\text{cyclic}}$, $C_{20,\text{star:upper}}$, $C_{20,\text{star:lower}}$, and $C_{20,\text{chain}}$. Our analytic results shows $C_{20,\text{cyclic}}^{\text{Path}}(U_1, U_2) = C_{20,\text{chain}}^{\text{Path}}(U_1) + C_{20,\text{chain}}^{\text{Path}}(U_2)$ and $C_{20,\text{cyclic}}^{\text{Time}}(U_1, U_2) = C_{20,\text{chain}}^{\text{Time}}(U_1) + C_{20,\text{chain}}^{\text{Time}}(U_2)$, and $C_{20,\text{cyclic}}^{\text{Coupling}}(U_1, U_2) \approx C_{20,\text{chain}}^{\text{Coupling}}(U_1) + C_{20,\text{chain}}^{\text{Coupling}}(U_2)$. In a graphic description,

$$\begin{array}{cccc}
 C_{20,\text{cyclic}} & C_{20,\text{chain}}^{\text{Path}} & C_{20,\text{chain}}^{\text{Coupling}} & C_{20,\text{chain}}^{\text{Time}} \\
 \begin{array}{c} \text{Diagram of } C_{20,\text{cyclic}} \end{array} & = & \begin{array}{c} \text{Diagram of } C_{20,\text{chain}}^{\text{Path}} \\ + \\ \text{Diagram of } C_{20,\text{chain}}^{\text{Coupling}} \end{array} & + & \begin{array}{c} \text{Diagram of } C_{20,\text{chain}}^{\text{Time}} \end{array}
 \end{array}$$

It indicates that $C_{20,\text{cyclic}}$ in the treatment of ME fulfills the superposition law. Fig. 2 (b2) shows the numerical results for $C_{20,\text{cyclic}}$ coincide with the analytic ones, confirming the validity of superposition law. Although $C_{20,\text{star:upper}}$ and $C_{20,\text{star:lower}}$ in Fig. 2 (b3) are produced from the same formula according to similar structures, there is a bigger gap between numerical solution and ME result for the lower correlation than for the upper correlation. Due to $U_1 > U_2$, the large U_1 is involved more with $C_{20,\text{star}}^{\text{Coupling}}$ in the $C_{20,\text{star:lower}}$ and high-order terms in ME become more important than U_2 so dropping these terms lead to more derivation from exact results. The coincidence between numerics and analytics in Fig. 2 (b4) implies that the effect of $C_{R=2}^{\text{Coupling}}$ in the symmetric geometry is suppressed, in distinction to the asymmetric ge-

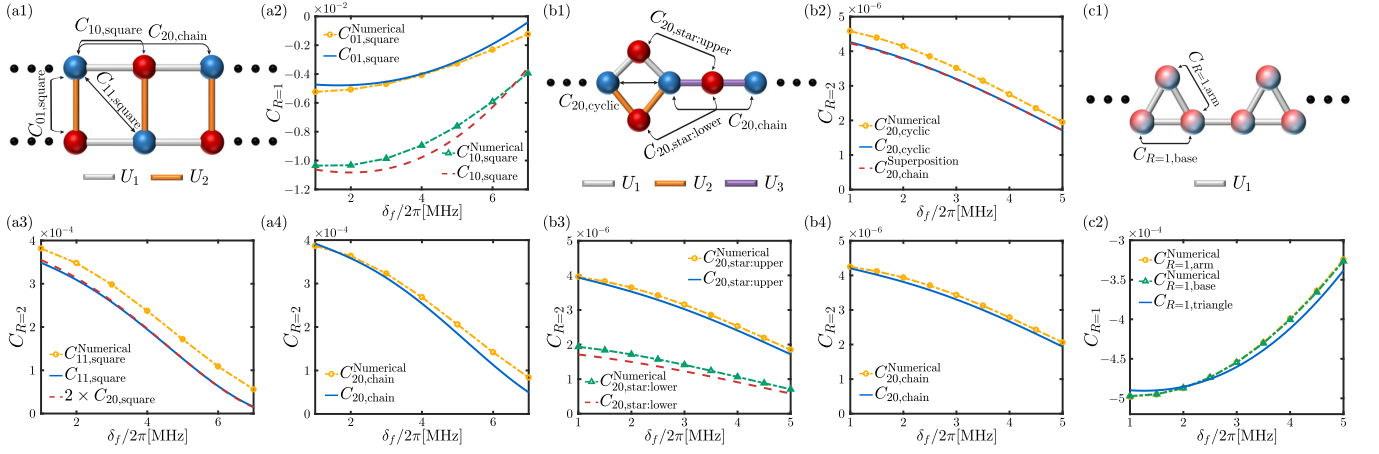


FIG. 2. The buildup of antiferromagnetic correlation on different lattices. Schematic description of $2 \times n$ lattice (a1), cyclic lattice with star (b1), and triangular lattice (c1). The nearest-neighbor correlations $C_{R=1}$ [(a2) and (c2)] and the next-nearest-neighbor correlations $C_{R=2}$ [(a3), (a4), (b2), (b3), and (b4)] as the function of δ_f . The yellow dotted lines with circle and the green dotted lines with triangle are produced by the results of numerically solving Schrödinger equation for Hamiltonian (1). The blue solid lines and red dashed lines show the analytic results of the corresponding correlation functions on the local lattice geometries.

ometry in Fig. 2 (b3) where the coupling effect is significantly important.

To check the validity of ME for more complex structures, we probe the nearest-neighbor AF correlation in the triangular lattice geometry – a frustrated magnetic system [see Fig. 2 (c1)]. Frustrated magnetic phenomena is macroscopic manifestation of many-body physics where the mixture effect of the degenerate quantum state leads to macroscopically the AF correlation. Frustrated magnets display exotic phases of matter, e.g., spin liquids, in which spins disorder but remain liquid-like due to strong quantum fluctuations even at absolute zero temperature. Spin liquid is a promising candidate in quantum communication and computation due to its properties, such as long-range entanglement and fractional quantum excitations [33]. Thus, the study of frustrated magnet is critical, which enhances deep understanding of fundamental physics and holds potential for the development in advanced material and techniques. From the analytic calculation, we acquire the selfsame expressions of the nearest-neighbor correlation from any two atoms in this triangle, where the terms from the shortest path and the mutual effect of Hamiltonian at different times are consistent with the ones in $2 \times n$ lattice, i.e., $C_{R=1, \text{triangle}}^{\text{Path}} = C_{10, \text{square}}^{\text{Path}}$, and $C_{R=1, \text{triangle}}^{\text{Time}} = C_{10, \text{square}}^{\text{Time}}$. Fig. 2 (c2) shows that the ME results agree basically with numerical calculation. Although the evolution of the degenerate quantum states is complex in the frustrated magnetic system, the ME can still give quantitative description for the buildup of the AF correlation. Moreover, $C_{R=1, \text{arm}}$ is approximately identical to $C_{R=1, \text{base}}$, indicating that the nearest-neighbor sites coupled to triangle sites affects trivially the buildup of AF correlation.

Figure 3 shows the connected correlation functions $C_{R=1}$ and $C_{R=2}$ vary with δ_f when the $2 \times n$ lattice system is subject to a quadratic modulation of detuning, i.e., $\delta(t) = \frac{\delta_f - \delta_0}{T^2} t^2 + \delta_0$. In contrast to the linear modulation of $\delta(t)$

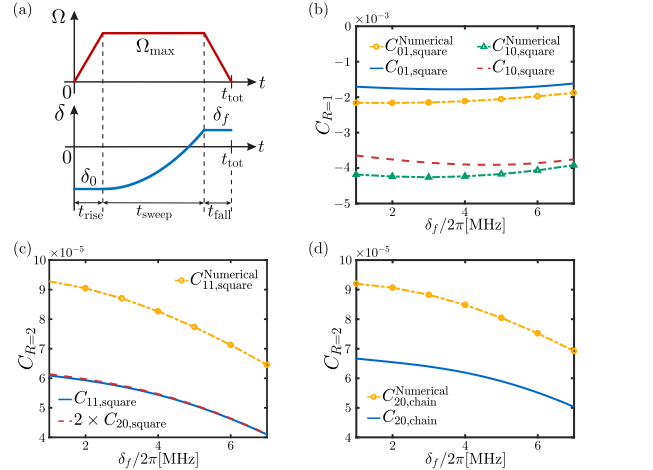


FIG. 3. The buildup of antiferromagnetic correlation with different quench process on $2 \times n$ lattice. (a) The Rabi frequency $\Omega(t)$ and the detuning $\delta(t)$ are modulated in top and bottom curves, respectively. (b) The nearest-neighbor correlation $C_{01, \text{square}}$ and $C_{10, \text{square}}$ and (c) the next-nearest-neighbor correlation $C_{11, \text{square}}$ and (d) $C_{20, \text{square}}$ as the function of δ_f .

shown in Fig. 2, the ME can still give quantitative description of $C_{R=1}$ despite it is qualitatively consistent with the numerical calculation for $C_{R=2}$. It indicates that for a different modulation of $\delta(t)$, our ME results up to the second-order is still valid for the quantum driven dynamics. Moreover, in Fig. 3 (c), the blue solid line overlaps nearly with red dashed line, $C_{11, \text{square}} = 2 \times C_{20, \text{square}}$, implying that the superposition law of the shortest paths for the AF correlation is independent of the quench style.

In summary, we investigate numerically and analytically the buildup of AF correlation in the nonuniform Ising-like system. We find the magnitude of the correlation between two refer-

ence points is sum of the correlation of all the shortest paths between two points – a typical superposition law. Such superposition law is independent of lattice geometries, more essentially nonequivalent paths, and quench style. It indicates that to probe an numerically inaccessible large and complex lattice system can be simplified into study the typical small units. We anticipate some potential applications of ME and similar mechanism of the buildup of inner correlations for other strongly correlated systems, such as Heisenberg model and Hubbard model.

We would like to thank Uwe R. Fischer and Jun-Hui Zheng for stimulating discussions. This work is supported by the National Natural Science Foundation of China under Grants No.12075175 and No.11775178.

* boxiong@whut.edu.cn

- [1] M. Rigol, V. Dunjko, and M. Olshanii, Thermalization and its mechanism for generic isolated quantum systems, *Nature (London)* **452**, 854 (2008).
- [2] J. Eisert, M. Friesdorf, and C. Gogolin, Quantum many-body systems out of equilibrium, *Nat. Phys.* **11**, 124 (2015).
- [3] B. Damski, The simplest quantum model supporting the kibble-zurek mechanism of topological defect production: Landau-Zener transitions from a new perspective, *Phys. Rev. Lett.* **95**, 035701 (2005).
- [4] W. H. Zurek, U. Dorner, and P. Zoller, Dynamics of a quantum phase transition, *Phys. Rev. Lett.* **95**, 105701 (2005).
- [5] J. Dziarmaga, Dynamics of a quantum phase transition: Exact solution of the quantum ising model, *Phys. Rev. Lett.* **95**, 245701 (2005).
- [6] R. Schützhold, M. Uhlmann, Y. Xu, and U. R. Fischer, Sweeping from the superfluid to the mott phase in the bose-hubbard model, *Phys. Rev. Lett.* **97**, 200601 (2006).
- [7] P. Calabrese and J. Cardy, Time dependence of correlation functions following a quantum quench, *Phys. Rev. Lett.* **96**, 136801 (2006).
- [8] V. Lienhard, S. de Léséleuc, D. Barredo, T. Lahaye, A. Browaeys, M. Schuler, L.-P. Henry, and A. M. Läuchli, Observing the space- and time-dependent growth of correlations in dynamically tuned synthetic ising models with antiferromagnetic interactions, *Phys. Rev. X* **8**, 021070 (2018).
- [9] K. Sengupta, S. Powell, and S. Sachdev, Quench dynamics across quantum critical points, *Phys. Rev. A* **69**, 053616 (2004).
- [10] P. Calabrese, F. H. L. Essler, and M. Fagotti, Quantum quench in the transverse-field ising chain, *Phys. Rev. Lett.* **106**, 227203 (2011).
- [11] E. Guardado-Sanchez, P. T. Brown, D. Mitra, T. Devakul, D. A. Huse, P. Schauf, and W. S. Bakr, Probing the quench dynamics of antiferromagnetic correlations in a 2d quantum ising spin system, *Phys. Rev. X* **8**, 021069 (2018).
- [12] H. Labuhn, D. Barredo, S. Ravets, S. de Léséleuc, T. Macrì, T. Lahaye, and A. Browaeys, Tunable two-dimensional arrays of single rydberg atoms for realizing quantum ising models, *Nature (London)* **534**, 667 (2016).
- [13] P. Scholl, M. Schuler, H. J. Williams, A. A. Eberharter, D. Barredo, K.-N. Schymik, V. Lienhard, L.-P. Henry, T. C. Lang, T. Lahaye, *et al.*, Quantum simulation of 2d antiferromagnets with hundreds of rydberg atoms, *Nature (London)* **595**, 233 (2021).
- [14] B. Swingle, G. Bentsen, M. Schleier-Smith, and P. Hayden, Measuring the scrambling of quantum information, *Phys. Rev. A* **94**, 040302(R) (2016).
- [15] R. Samajdar, W. W. Ho, H. Pichler, M. D. Lukin, and S. Sachdev, Quantum phases of rydberg atoms on a kagome lattice, *Proc. Natl. Acad. Sci.* **118**, e2015785118 (2021).
- [16] G. Semeghini, H. Levine, A. Keesling, S. Ebadi, T. T. Wang, D. Bluvstein, R. Verresen, H. Pichler, M. Kalinowski, R. Samajdar, *et al.*, Probing topological spin liquids on a programmable quantum simulator, *Science* **374**, 1242 (2021).
- [17] D. Bluvstein, A. Omran, H. Levine, A. Keesling, G. Semeghini, S. Ebadi, T. T. Wang, A. A. Michailidis, N. Maskara, W. W. Ho, S. Choi, M. Serbyn, M. Greiner, V. Vuletić, and M. D. Lukin, Controlling quantum many-body dynamics in driven rydberg atom arrays, *Science* **371**, 1355 (2021).
- [18] M. Kim, Y. Song, J. Kim, and J. Ahn, Quantum ising hamiltonian programming in trio, quartet, and sextet qubit systems, *PRX Quantum* **1**, 020323 (2020).
- [19] D. Barredo, S. de Léséleuc, V. Lienhard, T. Lahaye, and A. Browaeys, An atom-by-atom assembler of defect-free arbitrary two-dimensional atomic arrays, *Science* **354**, 1021 (2016).
- [20] A. Browaeys and T. Lahaye, Many-body physics with individually controlled rydberg atoms, *Nat. Phys.* **16**, 132 (2020).
- [21] S. Weber, C. Tresp, H. Menke, A. Urvoy, O. Firstenberg, H. P. Büchler, and S. Hofferberth, Calculation of rydberg interaction potentials, *J. Phys. B: At. Mol. Opt. Phys.* **50**, 133001 (2017).
- [22] S. Ravets, H. Labuhn, D. Barredo, T. Lahaye, and A. Browaeys, Measurement of the angular dependence of the dipole-dipole interaction between two individual rydberg atoms at a förster resonance, *Phys. Rev. A* **92**, 020701 (2015).
- [23] B. Buča, Unified theory of local quantum many-body dynamics: Eigenoperator thermalization theorems, *Phys. Rev. X* **13**, 031013 (2023).
- [24] S. Blanes, F. Casas, J. A. Oteo, and J. Ros, The magnus expansion and some of its applications, *Phys. Rep.* **470**, 151 (2009).
- [25] D. Baye and P.-H. Heenen, A theoretical study of fast proton-atomic hydrogen scattering, *J. Phys. B* **6**, 105 (1973).
- [26] I. Schek, J. Jortner, and M. L. Sage, Application of the magnus expansion for high-order multiphoton excitation, *Chem. Phys.* **59**, 11 (1981).
- [27] J. S. Waugh, Theory of broadband spin decoupling, *J. Magn. Reson.* **50**, 30 (1982).
- [28] H. D. Dahmen, B. Scholz, and F. Steiner, Infrared dynamics of quantum electrodynamics and the asymptotic behavior of the electron form factor, *Nuclear Phys. B* **202**, 365 (1982).
- [29] J. C. D’Olivo and J. A. Oteo, Magnus expansion and the two-neutrino oscillations in matter, *Phys. Rev. D* **42**, 256 (1990).
- [30] See the Supplemental Material for the details of the derivation of the effective two-level system, the self-consistency of ME, the analytic results for different lattice geometries, and the quadratic quench.
- [31] X. Wang, B. Yang, B. Zhang, and B. Xiong, Path-dependent correlations in dynamically tuned ising models and its short-time behavior: application of magnus expansion, *Phys. Lett. A* **519**, 129698 (2024).
- [32] W. H. Press, S. A. Teukolsky, W. T. Vetterling, and B. P. Flannery, *Numerical recipes in fortran 77: The art of scientific computing* (Cambridge University Press, 1992).
- [33] J. Wen, S.-L. Yu, S. Li, W. Yu, and J.-X. Li, Experimental identification of quantum spin liquids, *npj Quantum Mater.* **4**, 12 (2019).

Supplemental Material

This supplemental material is organized as follows. We first introduce a two-photon transition scheme and derive the effective two-level system. Then, we prove the self-consistency of Magnus expansion in detail. Third, we show the analytic expressions for different lattice geometries. Finally, we show the relation between quadratic quench and linear quench.

The effective two-level system

The effective Hamiltonian is deduced from the following equations,

$$\begin{array}{c} \text{---} |r\rangle \\ \text{---} \delta_r \\ \text{---} \Omega_r \\ \text{---} \delta_e \\ |e\rangle \\ \Omega_e \\ |g\rangle \end{array} \rightarrow \begin{array}{c} \text{---} |r\rangle \\ \text{---} \delta \\ |g\rangle \end{array} \quad \left(\begin{array}{cc} H & H_S \\ H_S & H \end{array} \right) \left(\begin{array}{c} P \\ Q \end{array} \right) = E \left(\begin{array}{c} P \\ Q \end{array} \right), \quad P + Q = 1. \quad (3)$$

We can obtain $H_{\text{eff}} = E = P^{-1}HP + P^{-1}H_SQQ^{-1}\frac{1}{E-H}QQ^{-1}H_S^T P$.

The ground state $|g\rangle$ is coupled to the intermediate state $|e\rangle$ with Rabi frequency Ω_e and detuning δ_e , and $|e\rangle$ is driven up to the excited state $|r\rangle$ with Rabi frequency Ω_r and detuning δ_r where $|\delta_e| \sim |\delta_r| \gg |\delta_t| = |\delta_e + \delta_r|$. The Hamiltonian of a three-level atom coupling to laser fields is given by ($\hbar = 1$),

$$H = \frac{\Omega_e}{2} (|g\rangle\langle e| + |e\rangle\langle g|) + \frac{\Omega_r}{2} (|e\rangle\langle r| + |r\rangle\langle e|) - \delta_e |e\rangle\langle e| - \delta_t |r\rangle\langle r|.$$

Corresponding to Eq. (3), the Hilbert space is divided into two parts, that is, the P subspace $P = P^{-1} = |g\rangle\langle g| + |r\rangle\langle r|$ and the Q subspace $Q = Q^{-1} = |e\rangle\langle e|$. Inserting H into H_{eff} , we obtain

$$\begin{aligned} P^{-1}HP &= -\delta_t |r\rangle\langle r|, & P^{-1}H_SQ &= \frac{\Omega_e}{2} |g\rangle\langle e| + \frac{\Omega_r}{2} |r\rangle\langle e|, \\ Q^{-1}\frac{1}{E-H}Q &= \frac{|e\rangle\langle e|}{\delta_e}, & Q^{-1}H_S^T P &= \frac{\Omega_e}{2} |e\rangle\langle g| + \frac{\Omega_r}{2} |e\rangle\langle r|. \end{aligned}$$

After rearranging, we have $H_{\text{eff}} = -\delta_t |r\rangle\langle r| + \frac{\Omega_e^2}{4\delta_e} |g\rangle\langle g| + \frac{\Omega_r^2}{4\delta_e} |r\rangle\langle r| + \frac{\Omega_e\Omega_r}{4\delta_e} (|g\rangle\langle r| + |r\rangle\langle g|)$. Due to $|g\rangle\langle g| + |r\rangle\langle r| = 1$, we obtain further,

$$H_{\text{eff}} = -\left(\delta_t + \frac{\Omega_e^2 - \Omega_r^2}{4\delta_e} \right) |r\rangle\langle r| + \frac{\Omega_e\Omega_r}{4\delta_e} (|g\rangle\langle r| + |r\rangle\langle g|),$$

where the effective detuning for two-level system $\delta = \delta_r + \frac{\Omega_e^2 - \Omega_r^2}{4\delta_e}$ and the effective Rabi frequency $\Omega = \frac{\Omega_e\Omega_r}{2\delta_e}$.

The self-consistency of Magnus expansion

To explore the nonequilibrium dynamics of the Rydberg atomic system, we employ Magnus expansion (ME) to derive analytic expression for some quantities, e.g., the connected correlation function, and compare it with exactly numerical solutions. As the $C_R(T)$ expression in main body of our paper, we can represent further the connected correlation function between the atom in $(0, 0)$ and the one in (ka, la) ,

$$C_R(T) = \langle \psi(T) | n_{(0,0)} n_{(k,l)} | \psi(T) \rangle - \langle \psi(T) | n_{(0,0)} | \psi(T) \rangle \langle \psi(T) | n_{(k,l)} | \psi(T) \rangle, \quad (4)$$

where the Manhattan distance $R = |k| + |l|$. As an approximate expansion, we need to verify ME fulfills some fundamental laws whether in each expansion or when all expansion levels are taken into account. For example, conventional wisdom has it that in absence of interaction, there does not exist any connected correlation, i.e., $C_R = 0$ for $U = 0$. In this part, we will give a rigorous proof that in the treatment of ME, its each level confirm $C_R = 0$ for $U = 0$. For convenience, we induce $\mathcal{L} = \langle \psi(T) | n_{(0,0)} n_{(k,l)} | \psi(T) \rangle$ and $L = \langle \psi(T) | n_{(0,0)} | \psi(T) \rangle \langle \psi(T) | n_{(k,l)} | \psi(T) \rangle$ in the correlation function $C_R(T)$. Since δ does not change the state, we begin to consider only the Ω term in a two-site system according to two-site connected correlation

function, i.e., $H = \frac{\Omega}{2}\sigma_1^x + \frac{\Omega}{2}\sigma_2^x$. Ω tends to flip the spin state so the excited state $|r\rangle$ occurs only when Ω^n with $n \in \text{odd}$ acts on the ground state $|g\rangle$. We can derive \mathcal{L} as,

$$\begin{aligned}\mathcal{L} &= \sum_{m,n \in \text{even}} \sum_{l,l'} \frac{(iT)^m}{(2l+1)!(m-2l-1)!} \frac{(-iT)^n}{(2l'+1)!(n-2l'-1)!} \left(\frac{\Omega}{2}\sigma_1^x\right)^{2l+1} \left(\frac{\Omega}{2}\sigma_2^x\right)^{m-2l-1} \left(\frac{\Omega}{2}\sigma_1^x\right)^{2l'+1} \left(\frac{\Omega}{2}\sigma_2^x\right)^{m-2l'-1} \\ &= \sum_{m,n=2} \frac{(iT)^m 2^{m-1}}{m!} \frac{(-iT)^n 2^{n-1}}{n!} \left(\frac{\Omega}{2}\sigma^x\right)^{m+n} \\ &= \sum_{m,n=2} \frac{(iT)^m}{m!} \frac{(-iT)^n}{n!} \frac{(\Omega\sigma^x)^{m+n}}{4}.\end{aligned}$$

Meanwhile, the term L is simplified into

$$L = \sum_{p,q,k,l=1} \frac{(iT)^p}{p!} \frac{(-iT)^q}{q!} \frac{(iT)^k}{k!} \frac{(-iT)^l}{l!} \frac{(\Omega\sigma)^{p+q+k+l}}{16},$$

where $p, q, k, l \geq 1$ and $p + q + k + l = m + n = N$.

To confirm $\mathcal{L} = L$, we need to prove

$$\sum_{m,n=2} \frac{4}{m!n!} = \sum_{p,q,k,l=1} \frac{(-1)^{q+l}}{p!q!k!l!}. \quad (5)$$

To expand both sides of the expression further, we have the left side

$$\sum_{m,n=2} \frac{4}{m!n!} = \frac{1}{N!} \sum_{m,n=2} \frac{4N!}{m!(N-m)!} = \frac{4}{N!} (2^{N-1} - 2) = \frac{1}{N!} (2^{N+1} - 8),$$

and the right side,

$$\begin{aligned}\sum_{p,q,k,l=1} \frac{(-1)^{q+l}}{p!q!k!l!} &= \sum_{m',n_e} \frac{1}{m'!n_e!} (2^{m'} - 2)(2^{n_e} - 2) - \sum_{m',n_o} \frac{1}{m'!n_o!} (2^{m'} - 2)(2^{n_o} - 2) \\ &= \sum_{n_e} \frac{1}{(N-n_e)!n_e!} (2^{N-n_e} - 2)(2^{n_e} - 2) - \sum_{n_o} \frac{1}{(N-n_o)!n_o!} (2^{N-n_o} - 2)(2^{n_o} - 2) \\ &= \frac{1}{N!} (2^{N+1} - 8),\end{aligned}$$

where $m' = p + k, n' = q + l, m' + n' = N$. Thus, Eq. (5) is proved and in each expansion level of ME, $C_R = 0$ for $U = 0$ when only Ω is taken into account.

Next, we consider the Hamiltonian including δ , $H = \frac{\Omega}{2}\sigma_1^x + \frac{\Omega}{2}\sigma_2^x - \delta n_1 - \delta n_2$. Due to $[\sigma_x, n] \neq 0$, H^m can not be decomposed into grid-dependent two parts, but we find that for any superposition $|\psi\rangle = a|g\rangle + b|r\rangle$ where $|a|^2 + |b|^2 = 1$, $\langle\psi|[\sigma_x, n]|\psi\rangle = 0$. So the Hamiltonian is divided into grid-dependent two parts,

$$H^m = \left(\frac{\Omega}{2}\sigma_1^x + \frac{\Omega}{2}\sigma_2^x - \delta n_1 - \delta n_2\right)^m = \sum_{l=1} C_m^l \left(\frac{\Omega}{2}\sigma_1^x - \delta n_1\right)^l \left(\frac{\Omega}{2}\sigma_2^x - \delta n_2\right)^{m-l} = \sum_{l=1} \frac{m!}{l!(m-l)!} \left(\frac{\Omega}{2}\sigma^x - \delta n\right)^m.$$

The corresponding two parts in the correlation function have the forms,

$$\mathcal{L} = \sum_{m,n} \frac{(iT)^m}{m!} \frac{(-iT)^n}{n!} (2^m - 2)(2^n - 2) \left(\frac{\Omega}{2}\sigma^x - \delta n\right)^N,$$

$$L = \sum_{p,q,k,l} \frac{(iT)^p}{p!} \frac{(-iT)^q}{q!} \frac{(iT)^k}{k!} \frac{(-iT)^l}{l!} (2^p - 2)(2^q - 2)(2^k - 2)(2^l - 2) \left(\frac{\Omega}{2}\sigma^x - \delta n\right)^N.$$

In a similar way to Eq. (5), the terms in \mathcal{L} and L can be expanded as

$$\sum_{m,n} \frac{1}{m!} \frac{1}{n!} (2^m - 2)(2^n - 2) = \frac{1}{N!} (2^{N+1} - 8),$$

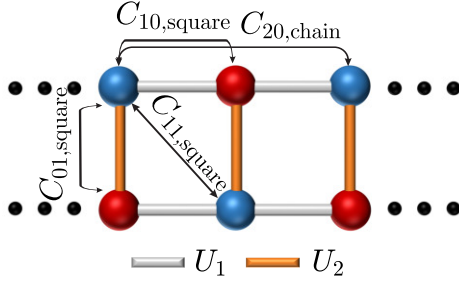
and

$$\begin{aligned} & \sum_{p,q,k,l} \frac{(iT)^p}{p!} \frac{(-iT)^q}{q!} \frac{(iT)^k}{k!} \frac{(-iT)^l}{l!} (2^p - 2)(2^q - 2)(2^k - 2)(2^l - 2) \\ &= \sum_{m',n'} \sum_{p,q} \frac{1}{p!(m'-p)!} \frac{(-1)^{n'}}{q!(n'-q)!} (2^{n'} - 2^q - 2^{n'-q} + 1) \\ &= \sum_{m',n'} (-1)^{n'} \frac{4^{m'} - 2 \times 3^{m'} + 2^{m'}}{m'!} \frac{4^{n'} - 2 \times 3^{n'} + 2^{n'}}{n'!} \\ &= \frac{1}{N!} (2^{N+1} - 8). \end{aligned}$$

Therefore, we obtain $\mathcal{L} = L$ for $U = 0$ for all expansion terms.

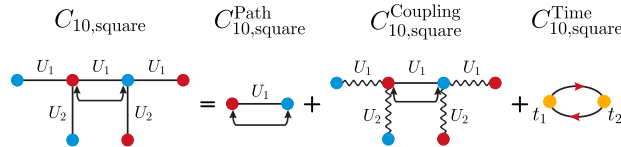
The analytic expressions for various geometries

According to the results of all kinds of local structures, we find a universal description for the standard terms: the denominator of all terms in these formulas can be simplified to $\Omega^p \delta^q U^m T^n$, where p, q, m, n are integer and $n = p + q + m$. The interaction U and detuning δ are variably involved in the most of terms, so we can extract the common factors that generally include T and Ω . Then we define a standard term as $\mathcal{M}_{(n,p)}^l$ for simply showing the analytic results, where l refers to the label of various local structures and n and p are the power numbers of T and Ω , respectively. The graphic descriptions about these local structures are shown as follows. The solid lines between two reference balls label the shortest paths and the wave lines denote the coupling from the nearest-neighbor sites to the shortest paths.



$2 \times n$ lattice – Here, we give more details about the analytic expressions of $2 \times n$ lattice that derived from the ME.

There are two types of the nearest-neighbor correlation, $C_{10,\text{square}}$ and $C_{01,\text{square}}$. We label them as a and b respectively.



(6)

the contribution from the shortest path is

$$C_{10,\text{square}}^{\text{Path}}(T) = -\frac{T^6 \Omega^4}{288} \mathcal{M}_{(6,4)}^a, \quad (7)$$

where

$$\mathcal{M}_{(6,4)}^a = [U_1(U_1 - 3\delta_{\text{avg}})],$$

the one from the nearest-neighbor coupling for the shortest path is

$$C_{10,\text{square}}^{\text{Coupling}}(T) = \frac{T^8 \Omega^4}{11520} \left[\mathcal{M}_{(8,4)}^a + \Omega^2 \mathcal{M}_{(8,6)}^a \right] - \frac{T^{10} \Omega^4}{4838400} \left[\mathcal{M}_{(10,4)}^a - \Omega^2 \mathcal{M}_{(10,6)}^a - \Omega^4 \mathcal{M}_{(10,8)}^a \right], \quad (8)$$

where

$$\begin{aligned} \mathcal{M}_{(8,4)}^a &= [U_1(U_1^3 - 6U_1^2\delta_{\text{avg}} + 15U_1\delta_{\text{avg}}^2 - 18\delta_{\text{avg}}^3)], \\ \mathcal{M}_{(8,6)}^a &= [2U_1(2U_1 - 5U_2 - 18\delta_{\text{avg}})], \\ \mathcal{M}_{(10,4)}^a &= [2U_1(U_1 - 3\delta_{\text{avg}})(3U_1^4 - 18U_1^3\delta_{\text{avg}} + 55U_1^2\delta_{\text{avg}}^2 - 84U_1\delta_{\text{avg}}^3 + 85\delta_{\text{avg}}^4)], \\ \mathcal{M}_{(10,6)}^a &= [550U_1^4 + 3U_1^3(65U_2 - 388\delta_{\text{avg}}) + U_1^2(293U_2^2 - 945U_2\delta_{\text{avg}} - 246\delta_{\text{avg}}^2) \\ &\quad + 5U_1(42U_2^3 - 209U_2^2\delta_{\text{avg}} + 376U_2\delta_{\text{avg}}^2 + 492\delta_{\text{avg}}^3)], \\ \mathcal{M}_{(10,8)}^a &= [U_1(674U_1 + 1505U_2 + 1950\delta_{\text{avg}})], \end{aligned}$$

and the one from the mutual effect of Hamiltonians at different times is

$$C_{10,\text{square}}^{\text{Time}}(T) = -\frac{T^8 \Omega^4}{20736} \left[1 + \frac{T^2}{288} (\delta_f - \delta_0)^2 \right] (\delta_f - \delta_0)^2 \mathcal{M}_{(6,4)}^a. \quad (9)$$

Considering the nearest-neighbor correlation in vertical direction,

$$\begin{array}{cccc} C_{01,\text{square}} & C_{01,\text{square}}^{\text{Path}} & C_{01,\text{square}}^{\text{Coupling}} & C_{01,\text{square}}^{\text{Time}} \\ \begin{array}{c} \text{Diagram 1: Square lattice with } U_1 \text{ and } U_2 \text{ couplings.} \end{array} & = & \begin{array}{c} \text{Diagram 2: Square lattice with } U_1 \text{ and } U_2 \text{ couplings, showing a path.} \end{array} & + & \begin{array}{c} \text{Diagram 3: Square lattice with } U_1 \text{ and } U_2 \text{ couplings, showing coupling.} \end{array} & + & \begin{array}{c} \text{Diagram 4: Two nodes } t_1 \text{ and } t_2 \text{ with a double-headed arrow.} \end{array} \end{array}, \quad (10)$$

three parts are corresponded to expressions as follows.

$$C_{01,\text{square}}^{\text{Path}}(T) = -\frac{T^6 \Omega^4}{288} \mathcal{M}_{(6,4)}^b, \quad (11)$$

where

$$\mathcal{M}_{(6,4)}^b = [U_1(U_1 - 3\delta_{\text{avg}})].$$

$$C_{01,\text{square}}^{\text{Coupling}}(T) = \frac{T^8 \Omega^4}{11520} \left[\mathcal{M}_{(8,4)}^b + \Omega^2 \mathcal{M}_{(8,6)}^b \right] - \frac{T^{10} \Omega^4}{4838400} \left[\mathcal{M}_{(10,4)}^b - \Omega^2 \mathcal{M}_{(10,6)}^b - \Omega^4 \mathcal{M}_{(10,8)}^b \right], \quad (12)$$

where

$$\begin{aligned} \mathcal{M}_{(8,4)}^b &= [U_1(U_1^3 - 6U_1^2\delta_{\text{avg}} + 15U_1\delta_{\text{avg}}^2 - 18\delta_{\text{avg}}^3)], \\ \mathcal{M}_{(8,6)}^b &= [2U_1(7U_1 - 10U_2 - 18\delta_{\text{avg}})], \\ \mathcal{M}_{(10,4)}^b &= [2U_1(U_1 - 3\delta_{\text{avg}})(3U_1^4 - 18U_1^3\delta_{\text{avg}} + 55U_1^2\delta_{\text{avg}}^2 - 84U_1\delta_{\text{avg}}^3 + 85\delta_{\text{avg}}^4)], \\ \mathcal{M}_{(10,6)}^b &= [-148U_1^4 + 2U_1^3(195U_2 + 413\delta_{\text{avg}}) + 2U_1^2(293U_2^2 - 945U_2\delta_{\text{avg}} - 1063\delta_{\text{avg}}^2) \\ &\quad + 10U_1(42U_2^3 - 209U_2^2\delta_{\text{avg}} + 376U_2\delta_{\text{avg}}^2 + 246\delta_{\text{avg}}^3)], \\ \mathcal{M}_{(10,8)}^b &= [U_1(-831U_1 + 3010U_2 + 1950\delta_{\text{avg}})]. \end{aligned}$$

$$C_{01,\text{square}}^{\text{Time}}(T) = -\frac{T^8 \Omega^4}{20736} \left[1 + \frac{T^2}{288} (\delta_f - \delta_0)^2 \right] (\delta_f - \delta_0)^2 \mathcal{M}_{(6,4)}^b. \quad (13)$$

Compared these expressions, we find that the contribution from the shortest path and the mutual effect of the Hamiltonian at different time are identical, which corresponded to the first and third terms in $C_{10,\text{square}}$ and $C_{01,\text{square}}$.

where

$$\mathcal{M}_{(10,6)}^d = [U_1^2(77U_1^2 - 340U_1\delta_{\text{avg}} + 375\delta_{\text{avg}}^2)].$$

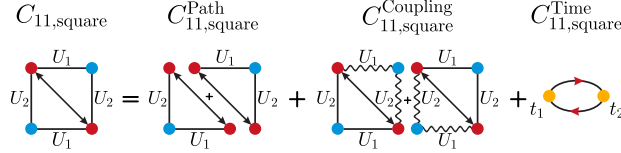
$$C_{20,\text{chain}}^{\text{Coupling}}(T) = -\frac{T^{12}\Omega^6}{29030400} [\mathcal{M}_{(12,6)}^d + \Omega^2 \mathcal{M}_{(12,8)}^d] + \frac{T^{14}\Omega^6}{26824089600} [\mathcal{M}_{(14,6)}^d - \Omega^2 \mathcal{M}_{(14,8)}^d - \Omega^4 \mathcal{M}_{(14,10)}^d], \quad (20)$$

where

$$\begin{aligned} \mathcal{M}_{(12,6)}^d &= [U_1^2(52U_1^4 - 368U_1^3\delta_{\text{avg}} + 1037U_1^2\delta_{\text{avg}}^2 - 1432U_1\delta_{\text{avg}}^3 + 831\delta_{\text{avg}}^4)], \\ \mathcal{M}_{(12,8)}^d &= [4U_1^2(U_1^2 - 143U_1\delta_{\text{avg}} + 318\delta_{\text{avg}}^2)], \\ \mathcal{M}_{(14,6)}^d &= [12U_1^2(121U_1^6 - 1170U_1^5\delta_{\text{avg}} + 4952U_1^4\delta_{\text{avg}}^2 - 11862U_1^3\delta_{\text{avg}}^3 + 17112U_1^2\delta_{\text{avg}}^4 \\ &\quad - 14322U_1\delta_{\text{avg}}^5 + 5565\delta_{\text{avg}}^6)], \\ \mathcal{M}_{(14,8)}^d &= [U_1^2(42405U_1^4 - 153388U_1^3\delta_{\text{avg}} + 102973U_1^2\delta_{\text{avg}}^2 + 165984U_1\delta_{\text{avg}}^3 - 222390\delta_{\text{avg}}^4)], \\ \mathcal{M}_{(14,10)}^d &= [6U_1^2(6347U_1^2 - 7868U_1\delta_{\text{avg}} - 25935\delta_{\text{avg}}^2)]. \end{aligned}$$

$$C_{20,\text{chain}}^{\text{Time}} = \frac{T^{12}\Omega^6}{116121600} \left[1 + \frac{T^2}{144}(\delta_f - \delta_0)^2 + \frac{T^4}{62208}(\delta_f - \delta_0)^4 \right] (\delta_f - \delta_0)^2 \mathcal{M}_{(10,6)}^d. \quad (21)$$

$C_{20,\text{square}}$ and $C_{20,\text{chain}}$ are identical if $U_2 = U_1$.



(22)

$$C_{11,\text{square}}^{\text{Path}}(T) = \frac{T^{10}\Omega^6}{4838400} \mathcal{M}_{(10,6)}^e, \quad (23)$$

where

$$\mathcal{M}_{(10,6)}^e = \{U_1U_2 [35(U_1^2 + U_2^2) + 238U_1U_2 - 680(U_1 + U_2)\delta_{\text{avg}} + 1500\delta_{\text{avg}}^2]\}.$$

$$C_{11,\text{square}}^{\text{Coupling}}(T) = -\frac{T^{12}\Omega^6}{58060800} [\mathcal{M}_{(12,6)}^e - \Omega^2 \mathcal{M}_{(12,8)}^e] + \frac{T^{14}\Omega^6}{53648179200} [\mathcal{M}_{(14,6)}^e - \mathcal{M}_{(14,8)}^e - \mathcal{M}_{(14,10)}^e], \quad (24)$$

where

$$\begin{aligned} \mathcal{M}_{(12,6)}^e &= \{U_1U_2 [12(U_1^4 + U_2^4) + 76(U_1^3U_2 + U_1U_2^3) + 32U_1^2U_2^2 - 254(U_1^3 + U_2^3)\delta_{\text{avg}} \\ &\quad - 482(U_1^2U_2 + U_1U_2^2)\delta_{\text{avg}} + 1183(U_1^2 + U_2^2)\delta_{\text{avg}}^2 + 1782U_1U_2\delta_{\text{avg}}^2 \\ &\quad - 2864(U_1 + U_2)\delta_{\text{avg}}^3 + 3324\delta_{\text{avg}}^4]\}, \\ \mathcal{M}_{(12,8)}^e &= \{U_1U_2 [356(U_1^2 + U_2^2) - 280U_1U_2 + 1144(U_1 + U_2)\delta_{\text{avg}} - 5088\delta_{\text{avg}}^2]\}, \\ \mathcal{M}_{(14,6)}^e &= \{U_1U_2 [154(U_1^6 + U_2^6) + 1056(U_1^5U_2 + U_1U_2^5) - 3864(U_1^5 + U_2^5)\delta_{\text{avg}} \\ &\quad + 26936(U_1^4 + U_2^4)\delta_{\text{avg}}^2 + 726(U_1^4U_2^2 + U_1^2U_2^4) - 10410(U_1^4U_2 + U_1U_2^4)\delta_{\text{avg}} \\ &\quad + 1936U_1^3U_2^3 - 13806(U_1^3U_2^2 + U_1^2U_2^3)\delta_{\text{avg}} + 58102(U_1^3U_2 + U_1U_2^3)\delta_{\text{avg}}^2 \\ &\quad - 103908(U_1^3 + U_2^3)\delta_{\text{avg}}^3 - 180780(U_1^2U_2 + U_1U_2^2)\delta_{\text{avg}}^3 + 241458(U_1^2 + U_2^2)\delta_{\text{avg}}^4 \\ &\quad - 343728(U_1 + U_2)\delta_{\text{avg}}^5 + 67620U_1^2U_2^2\delta_{\text{avg}}^2 + 338460U_1U_2\delta_{\text{avg}}^4 + 267120\delta_{\text{avg}}^6]\}, \\ \mathcal{M}_{(14,8)}^e &= \{U_1U_2 [32879(U_1^4 + U_2^4) + 70950(U_1^3U_2 + U_1U_2^3) - 155848(U_1^3 + U_2^3)\delta_{\text{avg}} \\ &\quad - 339944(U_1^2U_2 + U_1U_2^2)\delta_{\text{avg}} + 192850(U_1^2 + U_2^2)\delta_{\text{avg}}^2 + 331968(U_1 + U_2)\delta_{\text{avg}}^3 \\ &\quad + 120142U_1^2U_2^2 + 298844U_1U_2\delta_{\text{avg}}^2 - 889560\delta_{\text{avg}}^4]\}, \\ \mathcal{M}_{(14,10)}^e &= \{U_1U_2 [143682(U_1^2 + U_2^2) - 94416(U_1 + U_2)\delta_{\text{avg}} + 42372U_1U_2 \\ &\quad - 622440\delta_{\text{avg}}^2]\}. \end{aligned}$$

$$C_{11,\text{square}}^{\text{Time}}(T) = \frac{T^{12}\Omega^6}{232243200} \left[1 + \frac{T^2}{144}(\delta_f - \delta_0)^2 + \frac{T^4}{62208}(\delta_f - \delta_0)^4 \right] (\delta_f - \delta_0)^2 \mathcal{M}_{(10,6)}^e. \quad (25)$$

For $C_{20,\text{square}}$ and $C_{11,\text{square}}$, we find that $C_{11,\text{square}}^{\text{Path}}$ and $C_{11,\text{square}}^{\text{Time}}$ are certainly doubled $C_{20,\text{square}}^{\text{Path}}$ and $C_{20,\text{square}}^{\text{Time}}$ accordingly. For the second term, $C_{11,\text{square}}^{\text{Coupling}}$ is approximately twice $C_{20,\text{square}}^{\text{Coupling}}$ except there are slightly difference of coefficients in few terms.

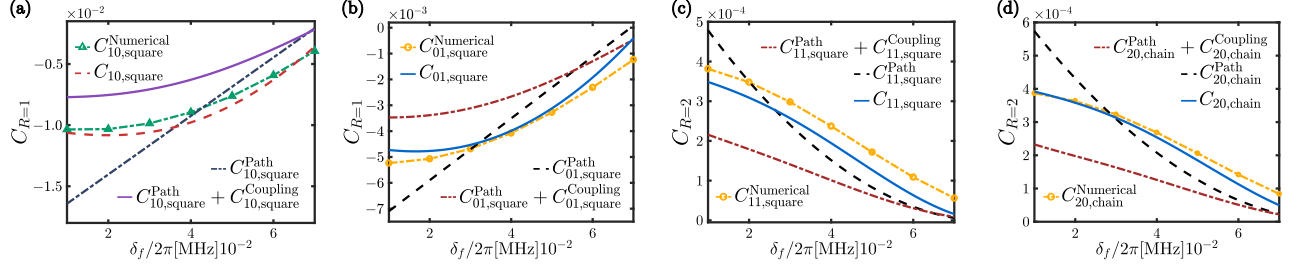
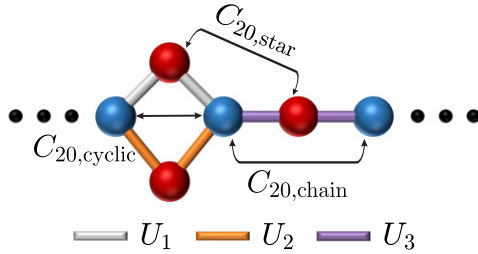


FIG. 4. The nearest-neighbor correlations, (a) $C_{10,\text{square}}$ and (b) $C_{01,\text{square}}$ and the next-nearest-neighbor correlations, (c) $C_{20,\text{chain}}$ and (d) $C_{11,\text{square}}$ as the function of δ_f in $2 \times n$ lattice.

Figure 4 shows that our analytic results, $C_{10,\text{square}}$, $C_{01,\text{square}}$, $C_{20,\text{chain}}$ and $C_{11,\text{square}}$ in accordance with the local lattice arrays match well the exactly numerical results for the $2 \times n$ lattice. It implies that in a short-time regime, the buildup of the local correlation in the large-scale lattice system is determined predominantly by the local lattice geometry around the correlated sites. Meanwhile, with increasing δ_f , the antiferromagnetic (AF) correlations are suppressed gradually. Since C_R^{Path} only agrees with the tendency of the numerical results, the leading approximation of ME can not describe precisely the AF correlation. When C_R^{Coupling} is taken into account, the variation of ME result is identical to the exactly numerical results, demonstrating $C_R^{\text{Path}} + C_R^{\text{Coupling}}$ can describe qualitatively the buildup of the AF correlation in the nonequilibrium dynamics. Yet when we consider the term of C_R^{Time} , the ME results can quantitatively describe the connected correlation function. Also the analytic expression shows for fixed T , Ω , δ_f , the larger U , the larger $C_{R=1}$, so the AF correlation between horizontal sites is larger than the one between vertical sites.



Cyclic lattice with star – There are specific analytic expression of cyclic lattice with star. We mainly consider three types of the next-nearest-neighbor correlation, i.e., $C_{20,\text{cyclic}}$ and $C_{20,\text{star}}$ in this model. f and g are represented $C_{20,\text{cyclic}}$ and $C_{20,\text{star}}$, respectively. f' indicates $C_{20,\text{chain}}^{\text{Superposition}}$.

We first consider three terms in $C_{20,\text{cyclic}}$,

$$C_{20,\text{cyclic}} = C_{20,\text{cyclic}}^{\text{Path}} + C_{20,\text{cyclic}}^{\text{Coupling}} + C_{20,\text{cyclic}}^{\text{Time}}$$

(26)

$$C_{20,\text{cyclic}}^{\text{Path}}(T) = \frac{T^{10}\Omega^6}{2419200} \mathcal{M}_{(10,6)}^f, \quad (27)$$

where

$$\mathcal{M}_{(10,6)}^f = [77(U_1^4 + U_2^4) - 340(U_1^3 + U_2^3)\delta_{\text{avg}} + 375(U_1^2 + U_2^2)\delta_{\text{avg}}^2].$$

$$C_{20,\text{cyclic}}^{\text{Coupling}}(T) = -\frac{T^{12}\Omega^6}{58060800} \left[\mathcal{M}_{(12,6)}^f + \Omega^2 \mathcal{M}_{(12,8)}^f \right] + \frac{T^{14}\Omega^6}{53648179200} \left[\mathcal{M}_{(14,6)}^f + \Omega^2 \mathcal{M}_{(14,8)}^f + \Omega^4 \mathcal{M}_{(14,10)}^f \right], \quad (28)$$

where

$$\begin{aligned} \mathcal{M}_{(12,6)}^f &= [104(U_1^6 + U_2^6) - 736(U_1^5 + U_2^5)\delta_{\text{avg}} + 2074(U_1^4 + U_2^4)\delta_{\text{avg}}^2 - 2864(U_1^3 + U_2^3)\delta_{\text{avg}}^3 \\ &\quad + 1662(U_1^2 + U_2^2)\delta_{\text{avg}}^4], \\ \mathcal{M}_{(12,8)}^f &= \{593(U_1^4 + U_2^4) - 585(U_1^3U_2 + U_1U_2^3) - 448U_1^2U_2^2 \\ &\quad - 88(U_1 + U_2) [28(U_1^2 + U_2^2) - 43U_1U_2] \delta_{\text{avg}} + 2544(U_1^2 + U_2^2)\delta_{\text{avg}}^2\}, \\ \mathcal{M}_{(14,6)}^f &= \{24 [121(U_1^8 + U_2^8) - 1170(U_1^7 + U_2^7)\delta_{\text{avg}} + 4952(U_1^6 + U_2^6)\delta_{\text{avg}}^2 - 11862(U_1^5 + U_2^5)\delta_{\text{avg}}^3 \\ &\quad + 17112(U_1^4 + U_2^4)\delta_{\text{avg}}^4 - 14322(U_1^3 + U_2^3)\delta_{\text{avg}}^5 + 5565(U_1^2 + U_2^2)\delta_{\text{avg}}^6]\}, \\ \mathcal{M}_{(14,8)}^f &= \{11 [2771(U_1^6 + U_2^6) - 4060(U_1^5U_2 + U_1U_2^5) - 7893(U_1^4U_2^2 + U_1^2U_2^4) - 11436U_1^3U_2^3] \\ &\quad - 6(U_1 + U_2) [34742(U_1^4 + U_2^4) - 76315(U_1^3U_2 + U_1U_2^3) + 514U_1^2U_2^2] \delta_{\text{avg}} \\ &\quad + [577781(U_1^4 + U_2^4) - 538804(U_1^3U_2 + U_1U_2^3) - 762498U_1^2U_2^2] \delta_{\text{avg}}^2 \\ &\quad - 84(U_1 + U_2) [9397(U_1^2 + U_2^2) - 14842U_1U_2] \delta_{\text{avg}}^3 + 444780(U_1^2 + U_2^2)\delta_{\text{avg}}^4\}, \\ \mathcal{M}_{(14,10)}^f &= \{33 [2438(U_1^4 + U_2^4) - 5971(U_1^3U_2 + U_1U_2^3) - 2926U_1^2U_2^2] \\ &\quad - 21(U_1 + U_2) [15139(U_1^2 + U_2^2) - 34774U_1U_2] \delta_{\text{avg}} + 311220(U_1^2 + U_2^2)\delta_{\text{avg}}^2\}. \end{aligned}$$

$$C_{20,\text{cyclic}}^{\text{Time}}(T) = \frac{T^{12}\Omega^6}{116121600} \left[1 + \frac{T^2}{144}(\delta_f - \delta_0)^2 + \frac{T^4}{62208}(\delta_f - \delta_0)^4 \right] (\delta_f - \delta_0)^2 \mathcal{M}_{(10,6)}^f. \quad (29)$$

The expression of $C_{20,\text{chain}}^{\text{Superposition}}$ is divided into three parts, $C_{20,\text{chain}(U_1,U_2)}^{\text{Path}}$, $C_{20,\text{chain}(U_1,U_2)}^{\text{Coupling}}$ and $C_{20,\text{chain}(U_1,U_2)}^{\text{Time}}$.

$$C_{20,\text{chain}(U_1,U_2)}^{\text{Path}}(T) = \frac{T^{10}\Omega^6}{2419200} \mathcal{M}_{(10,6)}^{f'}, \quad (30)$$

where

$$\mathcal{M}_{(10,6)}^{f'} = [77(U_1^4 + U_2^4) - 340(U_1^3 + U_2^3)\delta_{\text{avg}} + 375(U_1^2 + U_2^2)\delta_{\text{avg}}^2].$$

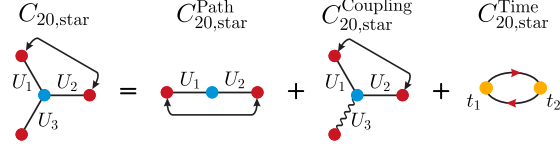
$$C_{20,\text{chain}(U_1,U_2)}^{\text{Coupling}}(T) = -\frac{T^{12}\Omega^6}{29030400} \left[\mathcal{M}_{(12,6)}^{f'} + \Omega^2 \mathcal{M}_{(12,8)}^{f'} \right] + \frac{T^{14}\Omega^6}{26824089600} \left[\mathcal{M}_{(14,6)}^{f'} - \Omega^2 \mathcal{M}_{(14,8)}^{f'} - \Omega^4 \mathcal{M}_{(14,10)}^{f'} \right], \quad (31)$$

where

$$\begin{aligned} \mathcal{M}_{(12,6)}^{f'} &= [52(U_1^6 + U_2^6) - 368(U_1^5 + U_2^5)\delta_{\text{avg}} + 1037(U_1^4 + U_2^4)\delta_{\text{avg}}^2 - 1432(U_1^3 + U_2^3)\delta_{\text{avg}}^3 \\ &\quad + 831(U_1^2 + U_2^2)\delta_{\text{avg}}^4], \\ \mathcal{M}_{(12,8)}^{f'} &= \{4 [(U_1^4 + U_2^4) - 143(U_1^3 + U_2^3)\delta_{\text{avg}} + 318(U_1^2 + U_2^2)\delta_{\text{avg}}^2]\}, \\ \mathcal{M}_{(14,6)}^{f'} &= \{12 [121(U_1^8 + U_2^8) - 1170(U_1^7 + U_2^7)\delta_{\text{avg}} + 4952(U_1^6 + U_2^6)\delta_{\text{avg}}^2 - 11862(U_1^5 + U_2^5)\delta_{\text{avg}}^3 \\ &\quad + 17112(U_1^4 + U_2^4)\delta_{\text{avg}}^4 - 14322(U_1^3 + U_2^3)\delta_{\text{avg}}^5 + 5565(U_1^2 + U_2^2)\delta_{\text{avg}}^6]\}, \\ \mathcal{M}_{(14,8)}^{f'} &= [42405(U_1^6 + U_2^6) - 153388(U_1^5 + U_2^5)\delta_{\text{avg}} + 102973(U_1^4 + U_2^4)\delta_{\text{avg}}^2 \\ &\quad + 165984(U_1^3 + U_2^3)\delta_{\text{avg}}^3 - 222390(U_1^2 + U_2^2)\delta_{\text{avg}}^4], \\ \mathcal{M}_{(14,10)}^{f'} &= \{6 [6347(U_1^4 + U_2^4) - 7868(U_1^3 + U_2^3)\delta_{\text{avg}} - 25935(U_1^2 + U_2^2)\delta_{\text{avg}}^2]\}. \end{aligned}$$

$$C_{20,\text{chain}(U_1,U_2)}^{\text{Time}}(T) = \frac{T^{12}\Omega^6}{116121600} \left[1 + \frac{T^2}{144}(\delta_f - \delta_0)^2 + \frac{T^4}{62208}(\delta_f - \delta_0)^4 \right] (\delta_f - \delta_0)^2 \mathcal{M}_{(10,6)}^{f'}. \quad (32)$$

Compared with the $C_{20,\text{chain}}^{\text{Superposition}}$, the sum of $C_{20,\text{chain}}$ under the two kinds of uniform interaction U_1 and U_2 , one can find that $C_{20,\text{cyclic}}^{\text{Path}}$ and $C_{20,\text{cyclic}}^{\text{Time}}$ fulfill the superposition principle. For $C_{20,\text{cyclic}}^{\text{Coupling}}$, the principle approximately is satisfied although there are few crossed terms about U_1 and U_2 .



(33)

$$C_{20,\text{star}}^{\text{Path}}(T) = \frac{T^{10}\Omega^6}{9676800}\mathcal{M}_{(10,6)}^g, \quad (34)$$

where

$$\mathcal{M}_{(10,6)}^g = \{U_1U_2 [35(U_1^2 + U_2^2) + 238U_1U_2 - 680(U_1 + U_2)\delta_{\text{avg}} + 1500\delta_{\text{avg}}^2]\}.$$

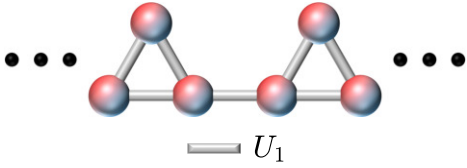
$$C_{20,\text{star}}^{\text{Coupling}}(T) = -\frac{T^{12}\Omega^6}{232243200} [\mathcal{M}_{(12,6)}^g + \Omega^2\mathcal{M}_{(12,8)}^g] + \frac{T^{14}\Omega^6}{214592716800} [\mathcal{M}_{(14,6)}^g + \Omega^2\mathcal{M}_{(14,8)}^g + \Omega^4\mathcal{M}_{(14,10)}^g], \quad (35)$$

where

$$\begin{aligned} \mathcal{M}_{(12,6)}^g &= U_1U_2 \{8 [3(U_1^4 + U_2^4) + 19(U_1^3U_2 + U_1U_2^3) + 8U_1^2U_2^2] \\ &\quad - 4(U_1 + U_2) [127(U_1^2 + U_2^2) + 114U_1U_2] \delta_{\text{avg}} + 2 [1183(U_1^2 + U_2^2) + 1782U_1U_2] \delta_{\text{avg}}^2 \\ &\quad - 5728(U_1 + U_2)\delta_{\text{avg}}^3 + 6648\delta_{\text{avg}}^4\}, \\ \mathcal{M}_{(12,8)}^g &= U_1U_2 \{293(U_1^2 + U_2^2) - 126(U_1U_3 + U_2U_3) + 1786U_1U_2 \\ &\quad - 112 [44(U_1 + U_2) - 5U_3] \delta_{\text{avg}} + 10176\delta_{\text{avg}}^2\}, \\ \mathcal{M}_{(14,6)}^g &= 4U_1U_2 \{77(U_1^6 + U_2^6) + 528(U_1^5U_2 + U_1U_2^5) + 363(U_1^4U_2^2 + U_1^2U_2^4) + 968U_1^3U_2^3 \\ &\quad - [1932(U_1^5 + U_2^5) + 5205(U_1^4U_2 + U_1U_2^4) + 6903(U_1^3U_2^2 + U_1^2U_2^3)] \delta_{\text{avg}} \\ &\quad + [13468(U_1^4 + U_2^4) + 29051(U_1^3U_2 + U_1U_2^3) + 33810U_1^2U_2^2] \delta_{\text{avg}}^2 \\ &\quad - [51954(U_1^3 + U_2^3) + 90390(U_1^2U_2 + U_1U_2^2)] \delta_{\text{avg}}^3 \\ &\quad + [120729(U_1^2 + U_2^2) + 169230U_1U_2] \delta_{\text{avg}}^4 - 171864(U_1 + U_2)\delta_{\text{avg}}^5 + 133560\delta_{\text{avg}}^6\}, \\ \mathcal{M}_{(14,8)}^g &= U_1U_2 \{7700(U_1^4 + U_2^4) + 43549(U_1^3U_2 + U_1U_2^3) - 4235U_1^3U_3 - 4158U_1U_3^3 \\ &\quad + 19426U_1^2U_2^2 - 4851U_1^2U_3^2 - 9625(U_1^2U_2 + U_1U_2^2)U_3 - 13134U_1U_2U_3^2 - [142604U_1^3 \\ &\quad + 274300(U_1^2U_2 + U_1U_2^2) - 43547U_1^2U_3 - 48930U_1U_3^2 - 69818U_1U_2U_3] \delta_{\text{avg}} + (647717U_1^2 \\ &\quad + 1015690U_1U_2 - 161700U_1U_3)\delta_{\text{avg}}^2 - 1578696U_1\delta_{\text{avg}}^3 - 7 [11U_2(55U_2^2U_3 + 63U_2U_3^2 + 54U_3^3) \\ &\quad - (20372U_2^3 - 6221U_2^2U_3 - 6990U_2U_3^2 - 2520U_3^3)]\delta_{\text{avg}} + (92531U_2^2 - 23100U_2U_3 \\ &\quad - 14844U_3^2)\delta_{\text{avg}}^2 - 24(9397U_2 - 1475U_3)\delta_{\text{avg}}^3 + 254160\delta_{\text{avg}}^4\}, \\ \mathcal{M}_{(14,10)}^g &= U_1U_2 \{7 [5973(U_1^2 + U_2^2) - 6248U_3(U_1 + U_2)] + 238194U_1U_2 \\ &\quad - 7 [90834(U_1 + U_2) - 27300U_3] \delta_{\text{avg}} + 1244880\delta_{\text{avg}}^2\}. \end{aligned}$$

$$C_{20,\text{star}}^{\text{Time}}(T) = \frac{T^{12}\Omega^6}{464486400} \left[1 + \frac{T^2}{144}(\delta_f - \delta_0)^2 + \frac{T^4}{62208}(\delta_f - \delta_0)^4 \right] (\delta_f - \delta_0)^2 \mathcal{M}_{(10,6)}^g. \quad (36)$$

As mentioned above, $C_{20,\text{star}}^{\text{Path}}$ and $C_{20,\text{star}}^{\text{Time}}$ are identical respectively with $C_{20,\text{square}}^{\text{Path}}$ and $C_{20,\text{square}}^{\text{Time}}$ due to the same shortest paths of them.



Triangular lattice – The analytic results of triangular lattice that derived from the ME show as follows. The expressions of the nearest-neighbor correlation between any two atoms in the triangle are identical. We denote this model as h .

$$C_{R=1,\text{triangle}} = C_{R=1,\text{triangle}}^{\text{Path}} + C_{R=1,\text{triangle}}^{\text{Coupling}} + C_{R=1,\text{triangle}}^{\text{Time}}$$

(37)

where the contribution from the shortest path is

$$C_{R=1,\text{triangle}}^{\text{Path}}(T) = -\frac{T^6 \Omega^4}{288} \mathcal{M}_{(6,4)}^h, \quad (38)$$

where

$$\mathcal{M}_{(6,4)}^h = [U_1(U_1 - 3\delta_{\text{avg}})],$$

the one from the nearest-neighbor coupling is

$$C_{R=1,\text{triangle}}^{\text{Coupling}}(T) = \frac{T^8 \Omega^4}{11520} [\mathcal{M}_{(8,4)}^h + \Omega^2 \mathcal{M}_{(8,4)}^h] - \frac{T^{10} \Omega^4}{2419200} [\mathcal{M}_{(10,4)}^h - \Omega^2 \mathcal{M}_{(10,6)}^h - \Omega^4 \mathcal{M}_{(10,8)}^h], \quad (39)$$

where

$$\begin{aligned} \mathcal{M}_{(8,4)}^h &= [U_1(U_1^3 - 6U_1^2\delta_{\text{avg}} + 15U_1\delta_{\text{avg}}^2 - 18\delta_{\text{avg}}^3)], \\ \mathcal{M}_{(8,6)}^h &= [4U_1(U_1 - 9\delta_{\text{avg}})], \\ \mathcal{M}_{(10,4)}^h &= [U_1(U_1 - 3\delta_{\text{avg}})(3U_1^4 - 18U_1^3\delta_{\text{avg}} + 55U_1^2\delta_{\text{avg}}^2 - 84U_1\delta_{\text{avg}}^3 + 85\delta_{\text{avg}}^4)], \\ \mathcal{M}_{(10,6)}^h &= [2U_1(282U_1^3 - 631U_1^2\delta_{\text{avg}} + 126U_1\delta_{\text{avg}}^2 + 615\delta_{\text{avg}}^3)], \\ \mathcal{M}_{(10,8)}^h &= [U_1(337U_1 + 975\delta_{\text{avg}})], \end{aligned}$$

and one from the mutual effect of Hamiltonian at different times is

$$C_{R=1,\text{triangle}}^{\text{Time}}(T) = -\frac{T^8 \Omega^4}{20736} \left[1 + \frac{T^2}{288} (\delta_f - \delta_0)^2 \right] (\delta_f - \delta_0)^2 \mathcal{M}_{(6,4)}^h. \quad (40)$$

Similarly, $C_{R=1,\text{triangle}}^{\text{Path}}$ and $C_{R=1,\text{triangle}}^{\text{Time}}$ are respectively identical with C^{Path} and C^{Time} in the nearest-neighbor correlations of square lattice due to the same shortest path.

Quadratic quench

We also consider the quadratic modulation of the detuning, $\delta'(t) = \frac{\delta_f - \delta_0}{T^2} t^2 + \delta_0$. For the Hamiltonian $H = \frac{\Omega(t)}{2} \sum_i \sigma_i^x - \delta(t) \sum_i n_i + \sum_{\langle ij \rangle} U_{ij} n_i n_j$ ($\hbar = 1$), we can deduce by employing ME,

$$\bar{H}_1 = \frac{\Omega}{2} \sum_i \sigma_i^x - \delta_{\text{avg}} \sum_i n_i + \sum_{\langle ij \rangle} U_{ij} n_i n_j,$$

and

$$\bar{H}_2 = \frac{\Omega}{24} (\delta_f - \delta_0) T \sum_i \sigma_i^y.$$

We find that for both linear and quadratic modulations, \bar{H}_1 and \bar{H}_2 have the identical forms except $\delta_{\text{avg}} = \frac{2\delta_0 + \delta_f}{3}$ for the quadratic quench and $\delta_{\text{avg}} = \frac{\delta_0 + \delta_f}{2}$ for the linear modulation. Therefore, two quench styles can share the similar analytic solution for the correlation function.